Modeling Operational Modes of a Bipolar Vacuum Microelectronic Device

Andrew C. Madison, *Member, IEEE*, Charles B. Parker, *Member, IEEE*, Jeffrey T. Glass, *Senior Member, IEEE*, and Brian R. Stoner, *Senior Member, IEEE*

***Abstract*—Vacuum microelectronic devices (VMDs) designed for bipolar charge operation hold great promise for applications in radiation-intensive and high-temperature environments. This novel class of devices was first realized in a microelectromechanical platform leveraging integrated carbon nanotube field emitters and an addressable pentode structure for controlling electron-impact dynamics in Ar ambients. That proof of concept demands the development of basic numerical models to aid device optimization. We address this need in the form of a two-fluid model of carrier transport dynamics in a bipolar VMD (BVMD). The fluid model captures the behavior of operational modes demonstrated in previously reported devices. Moreover, this approach promises insight into potentially unforeseen pressure and frequency dependences of the BVMD platform.**

***Index Terms*—Collisional plasma, finite-element methods (FEMs), fluid modeling, microelectromechanical devices.**

I. Introduction

RECENT demonstrations of a bipolar vacuum microelectronic device (VMD) (BVMD) have sparked interest in simulating their fundamental principles of operation. While classic VMDs benefit from high carrier mobility, radiation hardness, and thermal stability, BVMDs have the added benefit of utilizing ions as well as electrons for signal transduction [1]. This new class of device has been proven but lacks a self-consistent model of charge carrier transport. The capability of simulating carrier generation and flow will be useful for optimizing the electrochemical dynamics and ultimately transferring this experimental platform into application.

The first MEMS-based BVMD reported utilized a carbon nanotube (CNT) field emission (FE) triode flanked by two biasing panels to form a microion source when operated under inert gas ambients [1]. Similar multipanel microscale ionization sources have been reported, each being fabricated through the PolyMUMPS foundry process [2]–[6].

Manuscript received March 20, 2012; accepted July 5, 2012. Date of publication August 20, 2012; date of current version September 21, 2012. This work was supported in part by NSF EAGER Grant ECCS-1147548, by ARO STIR Grant W911NF-10-1-0219, and by the RTI Fellows Program at RTI International. The review of this letter was arranged by Editor L. Selmi.

A. C. Madison, C. B. Parker, and J. T. Glass are with the Department of Electrical and Computer Engineering, Duke University, Durham, NC 27708 USA (e-mail: andrew.madison@duke.edu).

B. R. Stoner is with the Department of Electrical and Computer Engineering, Duke University, Durham, NC 27708 USA, and also with the Center for Materials and Electronics Technologies, RTI International, Research Triangle Park, NC 27709 USA.

Color versions of one or more of the figures in this letter are available online at http://ieeexplore.ieee.org.

Digital Object Identifier 10.1109/LED.2012.2208445

During operation of the BVMD, an electron extraction voltage is applied between the CNT-FE cathode and polysilicon gate; positive and negative biases, V_+ and V_-, respectively, are applied with opposing polarities relative to the gate. Meanwhile, the device anode biased with a variable potential $(V_{\rm in})$ relative to the gate. When $V_{\rm in}$ is negative (Mode 1), electrons are pulled from the CNT-FE source, through the extraction gate, and directly into the V_+ panel, while ions, generated upon electron impact of the ambient gas atoms, are drawn to the V_- panel and anode. In contrast, when $V_{\rm in}$ is positive (Mode 2), electrons accelerate across the device to the anode and into the V_+ panel, while ions are shunted into the V_- panel. The insets in Fig. 2(c) show a schematic view of the BVMD gate (left), V_+ and V_- bias panels (top and bottom), and the anode (right) during each operational mode.

In this letter, the theoretical basis for general BVMD operation at arbitrary frequency and pressure is outlined for a set of electron impact reactions. Upon this framework, a simple finite-element model (FEM) of a BVMD is demonstrated in order to elucidate nuances associated with known BVMD operational modes.

II. Theoretical Framework

In the multifluid model, the differential form of the advection equation describing the motion of the ith species can be written

$$\frac{\partial}{\partial t}(n_i) + \nabla \cdot \mathbf{j}_i = R_i \tag{1}$$

where $\mathbf{j}_i = -\nabla(D_i n_i) + q_i \mu_i n_i \nabla\phi$ and D_i and μ_i are the diffusivity and mobility transport coefficients of each carrier of charge q_i as computed from the Boltzmann energy distribution function corresponding to the energy regime of interest [7]. Note that q_i is negative for electrons and positive for ions. The source term R_i represents the sum of electron impact reactions involved in the model chemistry. Together with boundary conditions permitting influx and outflux of charge, (1) ensures charge conservation so that the total charge injected into the device is equivalent to the sum over all boundaries of charge leaving the device. This term originates directly from reaction cross section data and an energy distribution function, as indicated in (2) and (3)

$$R_i = \sum_j x_j k_j N_n n_i \tag{2}$$

where x_j is the mole fraction of excited gaseous product of reaction j, which proceeds with a forward rate of k_j and N_n is

0741-3106/$31.00 © 2012 IEEE

TABLE I
BASIC ELECTRON IMPACT REACTIONS UNDER AN AR AMBIENT

Type	Reaction	$\Delta\varepsilon$ (eV)
Surface	$Ar^* \rightarrow Ar$	0
Surface	$Ar^+ \rightarrow Ar$	0
Elastic	$Ar + e^- \rightarrow Ar + e^-$	0
Excitation	$Ar + e^- \rightarrow Ar^* + e^-$	11.5
Ionization	$Ar + e^- \rightarrow Ar^+ + 2e^-$	15.8
Ionization	$Ar^* + e^- \rightarrow Ar^+ + 2e^-$	4.43

the neutral gas density that is related to gas pressure by $N_n = 2.6 \times 10^{20}\ \mathrm{m^{-3} \cdot Pa^{-1}}$. An accurate description of the rate coefficients k_j requires knowledge of the energy distribution function $f(\varepsilon)$ and the respective total collisional cross section $\sigma_j(\varepsilon)$ [7], [8]

$$k_j = \left(\frac{2q_i}{m_i}\right)^{\frac{1}{2}} \int_0^\infty \varepsilon \sigma_j(\varepsilon) f(\varepsilon) d\varepsilon. \tag{3}$$

Depending on the energy regime of interest, $f(\varepsilon)$ corresponding to a given reaction can be approximated with a Maxwellian distribution; this greatly simplifies models that include electron and ion transport.

Energy flux throughout the device is accounted for in a formulation similar to (1) and (2). A summation of the carrier energy density time derivative, energy flux divergence, and charge convection is balanced by an energy sinking term $S_{i,\varepsilon}$ which is equivalent to the collisional power loss within the device

$$\frac{\partial}{\partial t}(n_{i,\varepsilon}) + \nabla \cdot \mathbf{\Gamma}_{i,\varepsilon} + (\nabla\phi) \cdot \mathbf{j}_i = S_{i,\varepsilon} \tag{4}$$

where $\mathbf{\Gamma}_{i,\varepsilon} = -\nabla(D_\varepsilon n_\varepsilon) + q_i \mu_\varepsilon n_\varepsilon \nabla\phi$ and D_ε and μ_ε are the energy diffusivity and mobility corresponding to the charge carrier specified by index i. Furthermore, collisional power loss is described in a form congruent with (2)

$$S_{i,\varepsilon} = \sum_j x_j k_j N_n n_i \Delta\varepsilon_j \tag{5}$$

where $\Delta\varepsilon_j$ is the energy threshold of reaction j.

Last, the Poisson equation, respective boundary conditions from the panels, and the space charge density describe the electric potential distribution within the device

$$\nabla^2\phi = -\frac{1}{\epsilon_0} \sum_i q_i n_i. \tag{6}$$

III. MODEL IMPLEMENTATION

The BVMD model presented herein was constructed using the Plasma Module offered by Comsol Multiphysics FEM software package. This FEM software was chosen for its flexibility in model specification and capability of coupling preloaded physical equation systems into a single model. Particular to the BVMD model, Comsol offers the flexibility of using custom expressions for collisional loss, as described in (4) and (5), in addition to the ability of defining transport coefficients and collisional cross section data for the surface and gas phase reactions summarized in Table I.

The open source Boltzmann solver, Bolsig+, was used to compute the frequency- and pressure-dependent electron mobilities μ_e from a two-term Boltzmann model as reported elsewhere [7]. The frequency dependence of the electron mobility is primarily responsible for any frequency effect observed in the BVMD simulation as the Einstein relations were used to approximate the electron diffusivity D_e as well as the electron energy mobility $\mu_{e,\varepsilon}$ and diffusivity $D_{e,\varepsilon}$ in the following way: $D_e = (2/3)(n_\varepsilon/n_e)\mu_\varepsilon$, $\mu_{e,\varepsilon} = (5/3)\mu_e$, and $D_{e,\varepsilon} = (2/3)(n_\varepsilon/n_e)\mu_{e,\varepsilon}$. Ion diffusivity and mobility were computed from the Maxwell–Stefan binary diffusion coefficients and Einstein relations, a default setting of the FEM software. However, these parameters may also be user specified as was done for electrons.

Operational mode switching in the BVMD was modeled as a response to a 1-MHz perturbation of electric potentials defined on specific boundaries of a rectangular geometry measuring 200 μm $\times$ 150 μm.

An electron influx equivalent to 1 μA was defined at the gate electrode to represent a steady source of electrons emitted from bundles of CNTs not included in the model; this 50-μm boundary was also set to an electric potential of 0 V and an energy density that ramped from 0 to 100 eV. The V_+, V_-, and anode panels were defined as 100-μm boundaries centered at the top, bottom, and right of the model geometry. To aid model convergence, the V_+ and V_- panel voltages were ramped over $\sim$3 μs with a hyperbolic tangent function from 0 to 100 and -100 V, respectively. Meanwhile, a pulse train of oscillating polarity was applied to the anode boundary at a frequency of 1 MHz. The neutral gas pressure was set to 13.3 Pa (100 mtorr), and the initial densities of all other species were set to 0 $\mathrm{cm^{-3}}$. Fig. 1 summarizes the perturbation waveform implemented in the simulation, while Fig. 2(a) and (b) shows the simulation geometry with respective boundaries highlighted.

The time-dependent simulation was carried out for 5 μs with 6.25-ns resolution on a desktop computer with a 2.66-GHz Intel Core 2 Duo processor and 4 GB of 1067-MHz DDR3 RAM, and computation time was on the order of 1 h.

IV. RESULTS

Simulation results for the model chemistry described earlier were found to capture the expected behavior of each operational mode of the BVMD. As shown in Fig. 2, electron trajectories flow from the gate electrode (left) directly into the V_+ panel in Mode 1 and across the device into the positively biased V_+ and anode panels in Mode 2 operation. During each operational mode, electron–Ar collisions contribute to a total power loss, defined in (4) and (5), and are plotted as grayscale surfaces in Fig. 2(a) and (b). Note that the total power losses for each mode, in Fig. 2(a) and (b), are plotted on the same grayscale and that Mode 2 exhibits far less power sinking than Mode 1. The ion density generated upon ionizing impact then moves in response to the electric field established by panel biases. Under Mode 1, ion current density is observed flowing from areas of high impact density (along electron paths) into the V_- *and* anode panels. In contrast, ion density sinks primarily into the V_- panel under Mode 2, an observation correlated with a reduction in ion

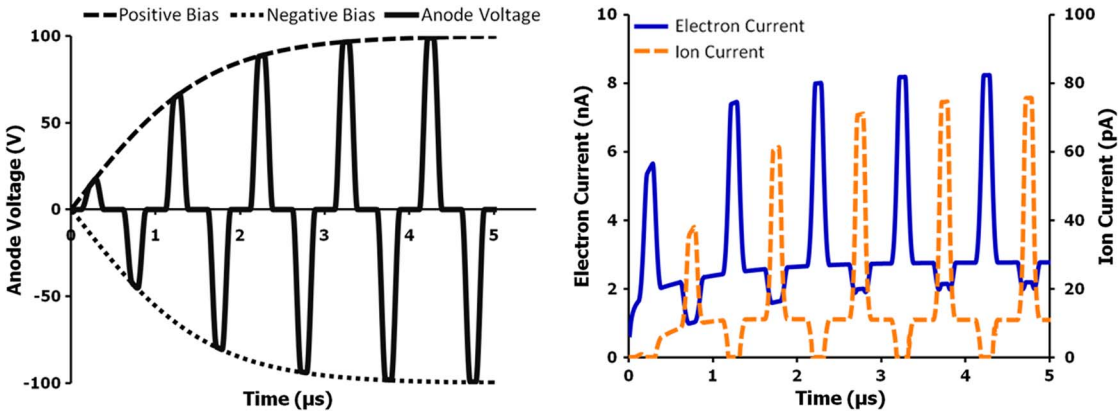

Fig. 1. (a) BVMD panel bias ramping along with anode pulse train profile. (b) Electron and ion current response computed for the anode panel.

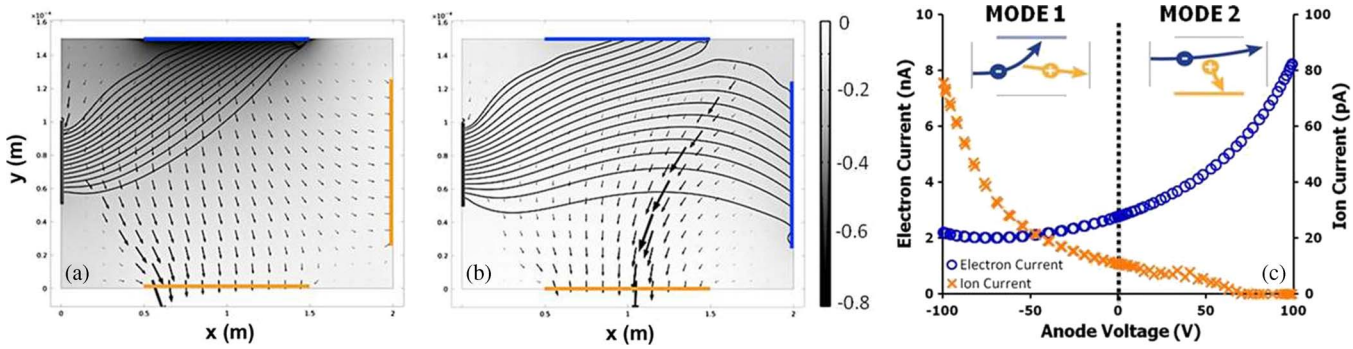

Fig. 2. BVMD fluid model simulation results. (a) and (b) show the collisional power density loss $(\mathrm{W} \cdot \mathrm{m}^{-2})$ (grayscale surface), electron current (streamlines), and total ion current (arrows) for Mode 1 and Mode 2, respectively. (c) I–V characteristic at the anode panel computed during operational mode switching. Note that, although electron and ion currents do impinge on multiple panels during BVMD operation, the I–V curve shown only reflects carrier flux at the *anode panel*.

current at the anode. Fig. 2(c) shows the voltage dependence of electron and ion currents at the anode for a BVMD with panels 50 μm tall in the $\hat{z}$-direction along with insets that indicate the primary flow of carriers during respective operational modes. For the pressure and frequency simulated, 13.3 Pa and 1 MHz, the ratio of Mode 1 electron current to Mode 2 ion current at the anode was found to be $\sim$100, an observation that parallels BVMD performance reported in [1].

These results carry several implications important to future refinement of BVMD theory and operation. First, that experimental observation was replicated suggests that the two-fluid modeling approach is a well-suited framework for describing BVMD operational modes. Additionally, the successful incorporation of frequency and pressure effects enables broader studies of BVMD performance; this notion demands for theoretical and experimental explorations of the frequency and pressure dependences of BVMD operation. The ability to track collisional power loss during mode switching as a function of frequency and pressure will lead to broader understanding of BVMD performance limitations.

V. Conclusion

A model of electron–argon impact chemistry and carrier transport has been applied to a novel BVMD geometry, and observational modes reported for actual devices were replicated *in silico*. Care was taken to incorporate frequency dependence into the BVMD model as externally calculated electron mobility. The model presented herein enables general studies of BVMD operation and should allow discovery of performance optima and overall design improvement.

References

[1] B. R. Stoner, J. R. Piascik, K. H. Gilchrist, C. B. Parker, and J. T. Glass, "A bipolar vacuum microelectronic device," *IEEE Trans. Electron Devices*, vol. 58, no. 9, pp. 3189–3194, Sep. 2011.

[2] C. A. Bower, K. H. Gilchrist, J. R. Piascik, B. R. Stoner, S. Natarajan, C. B. Parker, S. D. Wolter, and J. T. Glass, "On-chip electron-impact ion source using carbon nanotube field emitters," *Appl. Phys. Lett.*, vol. 90, no. 12, pp. 124102-1–124102-3, Mar. 2007.

[3] C. B. Natarajan, J. T. Parker, S. Glass, J. R. Piascik, K. H. Gilchrist, C. A. Bower, and B. R. Stoner, "High voltage microelectromechanical systems platform for fully integrated, on-chip, vacuum electronic devices," *Appl. Phys. Lett.*, vol. 92, no. 22, pp. 224101-1–224101-3, Jun. 2008.

[4] S. Natarajan, C. B. Parker, J. R. Piascik, K. H. Gilchrist, B. R. Stoner, and J. T. Glass, "Analysis of 3-panel and 4-panel microscale ionization sources," *J. Appl. Phys.*, vol. 107, no. 12, pp. 124508-1–124508-10, Jun. 2010.

[5] C. Bower, D. Shalom, W. Zhu, D. Lopez, G. P. Kochanski, P. L. Gammel, and S. Jin, "A micromachined vacuum triode using a carbon nanotube cold cathode," *IEEE Trans. Electron Devices*, vol. 49, no. 8, pp. 1478–1483, Aug. 2002.

[6] C. Bower, D. Shalom, W. Zhu, D. Lopez, L. H. Chen, P. L. Gammel, and S. Jin, "On-chip vacuum microtriode using carbon nanotube field emitters," *Appl. Phys. Lett.*, vol. 80, no. 20, pp. 3820–3822, May 2002.

[7] G. J. M. Hagelaar and L. C. Pitchford, "Solving the Boltzmann equation to obtain electron transport coefficients and rate coefficients for fluid models," *Plasma Sources Sci. Technol.*, vol. 14, no. 4, pp. 722–733, Nov. 2005.

[8] J. Dutton, "A survey of electron swarm data," *J. Phys. Chem. Ref. Data*, vol. 4, no. 3, pp. 577–856, Oct. 1975.